# Analysis of Magnetic Field Emissions in Inductive Power Transfer EV Chargers Following Reference Designs in SAE J2954/2019

Shi, Wenli; Grazian, Francesca; Dong, Jianning; Soeiro, Thiago Batista; Bauer, Pavol

**Important note**
To cite this publication, please use the final published version (if applicable).
Please check the document version above.

# Analysis of Magnetic Field Emissions in Inductive Power Transfer EV Chargers Following Reference Designs in SAE J2954/2019

Wenli Shi, Francesca Grazian, Jianning Dong, Thiago Batista Soeiro, and Pavol Bauer

Dept. Electrical Sustainable Energy, DCE&S group

TU Delft, Mekelweg 04, 2628 CD, Delft, the Netherlands

E-mail: W.Shi-3, F.Grazian, J.Dong-4, T.BatistaSoeiro, P.Bauer@tudelft.nl

*Abstract*—This paper aims to investigate the radiated magnetic field by 11 kW inductive power transfer (IPT) systems used for the charging of electric vehicles. Two reference designs suggested by SAE J2954 are studied. Both designs are analysed to obtain the coils winding currents, and 3D FEM models are built in COMSOL without considering the car chassis, which constitutes a conservative approach. The magnetic field intensity at specific distances from the IPT coupler are calculated. Finally, the simulation results are compared with the respective magnetic field limits defined in the international standards SAE J2954, IEC 61980-1 and ICNIRP. The results show that the magnetic field radiations at 10 meters points are significantly lower than the limits established in the SAE J2954, while the emissions at 0.9 meters points are only slightly below the limits defined by ICNIRP.

*Keywords — inductive power transfer, magnetic field radiation, reference designs, SAE J2954, ICNIRP, IPT standards*

## I. INTRODUCTION

In the next decade, inductive power transfer (IPT) technology is going to play an essential role in the charging of electric vehicles (EVs) [1], [2]. However, there are still some technical challenges, primarily related to the radiated magnetic field from the coupler of an IPT system [3]–[5]. For example, if the magnetic field is coupled with other electronic devices in the surroundings of the EV, it can cause malfunctioning. Besides, excessive magnetic field exposure may damage the health of living beings.

To make the IPT technology convenient to the users, the power level is continuously increased to shorten the charging time. However, in higher power, the winding current might generate a radiated magnetic field which exceeds the normalized limits. According to the standard SAE J2954, 82.8 dB ($\mu$A/m) is the recommended radiation limit for an 11 kW IPT systems operating at 85 kHz. As the polarity of the magnetic field is determined by the coil topology, the field emission changes among different couplers. In case the coils are unipolar, e.g., rectangular (D) coils, the magnetic field has a vertical orientation, as presented in Fig. 1(a). On the other hand, if the coils are bipolar, e.g., DD coils, the magnetic field has a horizontal orientation as shown in Fig. 1(b) [6], [7].

Although the first harmonics approximation (FHA) is widely used to analyse IPT systems, current harmonics should be considered in the research of radiated magnetic fields. A low radiation of the higher harmonic components of the magnetic field can be ensured by shaping the winding current as sinusoidal as possible, and thus, the design of the commonly employed compensation networks becomes essential. Compared with the basic compensations such as the series (S) compensation [8], [9], the LCC compensation provides winding current with less waveform distortion [10], [11].

In the norm SAE J2954 of April 2019, the reference designs of 11 kW IPT systems are updated. This paper aims to evaluate the magnetic field radiation of reference designs according to the limits issued by the norm. Both the circuit and finite element model (FEM) are implemented to analyse the winding current, coil arrangements and respective magnetic field emission. The results are compared to the norms SAE J2954 and IEC 61980-1.



(a) Rectangular coil
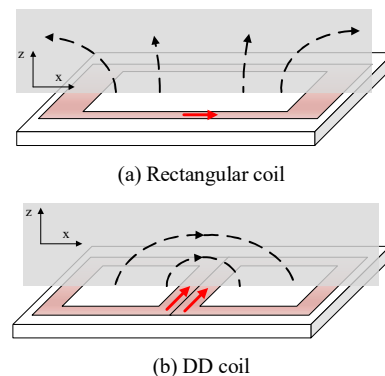


(b) DD coil

Figure 1. The magnetic field of the rectangular and DD coils.
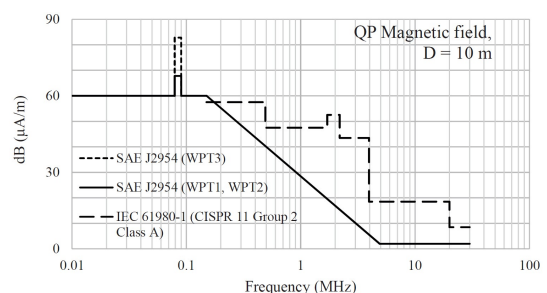


Figure 2. Limits of the magnetic field strength at 10 meters distance to the centre of the IPT coupler [12].

## II. INTERNATIONAL STANDARDS

### A. Electromagnetic Field Limits

Regarding the design requirements of the IPT systems, there are three available standards, which are the IEC 61980-1, ISO 19363 and SAE J2954 [12]. The IEC 61980 focuses on the general requirements of IPT systems, including electromagnetic field (EMF) exposure. The ISO 19363 and SAE J2954 elaborate on the design criteria of operation scenarios, physical dimensions, interoperability as well as the EMF exposure. The magnetic field strength limits defined in these three standards are summarized in [12], and they are

shown in Fig. 2. The curve limits of IEC 61980 is mostly above the one of SAE J2954, where the limits generally become critical as the frequency increases after 85 kHz. This makes it essential to check the magnetic field radiated by the fundamental component as well as the harmonics of the winding current. The magnetic field limits defined in the SAE J2954 is selected as the benchmark norm.

*B. Reference Design*

In SAE J2854, IPT systems are classified by the power level and air gap ranges that are presented in Table I. For applications below 7.7 kW, the first version of both SAE J2954 and ISO 19363 suggested reference designs for WPT1 and WPT2 using rectangular/circular or DD coil topologies. The latest version of SAE J2854 has been released in April 2019, and it updates the reference designs for the WPT3 applications. In each power level, three different vehicle assemblies (VAs) are illustrated for Z1, Z2, and Z3, respectively. The reference designs specify the physical dimensions and electrical parameters of the ground assembly (GA) and VA. Both GA and VA consist of the power converter, compensation circuit and charging pad, as shown in Fig. 3. The compensation topologies of both GA and VA use the LCC compensation because it possesses excellent robustness to the coupling variation and a winding current with fewer harmonics, which gives the LCC compensation an advantage. Regarding the coil topology, both rectangular and DD coils are popular. Thus, SAE J29854 provides reference designs for both coil topologies at all power levels and air gap ranges.

Since it is known that, in the main power transfer band, the magnetic field intensity increases when the source current rises, high-power IPT systems are more likely to exceed the EMF limits defined in the standards. Also, as the air gap increases, more leakage fields could be emitted. Therefore, reference designs of WPT3 and Z3 are selected as studied cases because they are the most critical situations.
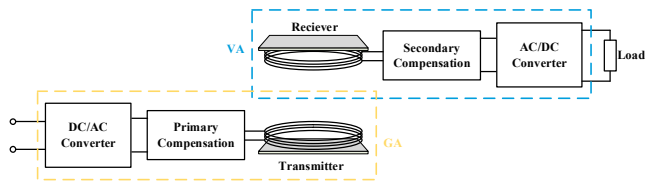


Figure 3. Definition of GA and VA.

TABLE I.        CLASSIFICATION OF IPT SYSTEM.

| Class | Power level / WPT (kW) | Air gap / Z (mm) |
|-------|------------------------|------------------|
| 1 | 3.7 | 100-150 |
| 2 | 7.7 | 140-210 |
| 3 | 11.1 | 170-250 |
| 4 | 22 | Not applicable |

III. MODELLING

The modelling method includes two parts. The first part is the circuit model that takes the electric specifications of the reference designs as input. The circuit simulations provide the winding current waveform with a high-resolution sampling data, such that the current harmonics in the MHz range can be accurately obtained. The other part is a FEM model that is built based on the mechanical specifications of

the reference designs. The current of the circuit model is taken as the input of the FEM model to compute the magnetic field radiation in the investigated frequency ranges.

*A. Assumptions*

In practice, IPT system parameters drift from the designed value due to the change of temperature, switching frequency as well as winding current. For simplicity, the model is built under the assumptions as follow:

- The winding AC resistances are constant.

- The winding self-inductance is equal to its value under 85 kHz.

- The compensation capacitors are ideal.

- The compensation inductors are ideal and have no contribution to the magnetic field radiation.

- The ferrite cores are not saturated and have constant permeability.

- The chassis of the car and other mechanical supports are not considered.

*B. Compensations*

The schematics of an IPT system using LCC/SP compensation are shown in Fig. 4. On the primary/transmitter side, there are three passive elements, a series capacitor $C_1$, a parallel capacitor $C_{f1,}$ and a series inductor $L_{f1}$. On the secondary/receiver side, one has a series capacitor $C_{s2}$ and a parallel capacitor $C_{p2}$ forming a SP compensation circuit. $V_{IN}$ and $V_{OUT}$ are the amplitude of inverter output and battery voltage, respectively. The parameters are designed as follow

$$j\omega_0 L_1 + \frac{1}{j\omega_0 C_1} + \frac{1}{j\omega_0 C_{f1}} = 0 \qquad (1)$$

$$j\omega_0 L_{f1} + \frac{1}{j\omega_0 C_{f1}} = 0 \qquad (2)$$

$$j\omega_0 L_2 + \frac{1}{j\omega_0 C_{s2}} + \frac{1}{j\omega_0 C_{p2}} = 0 \qquad (3)$$

where $\omega_0 = 2\pi f_0$ is the angular frequency for 85 kHz. It is noticed that the reflected impedance of the secondary side might not be purely resistive. To achieve zero phase angle operation of the primary power supply, $L_{f1}$ could be modified within the range recommended in the standard.
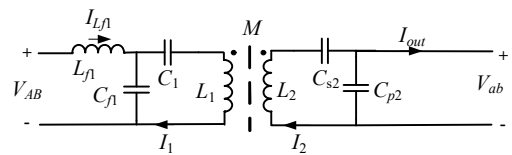


Figure 4. LCC/SP compensation circuit.

When the LCC/SP compensation works under resonance, the IPT system operates as a current source [13]. The fundamental output current $I_{out}$ can be calculated as

$$I_{out} = \frac{\omega_0 M C_{p2}}{j L_{f1}} V_{AB} \qquad (4)$$

where $M$ is the mutual inductance between $L_1$ and $L_2$. The output power is set to 11 kW. According to SAE J2854, the

electrical parameters designed for the WPT3 power level under the Z3 air gap are summarized in Table II.

TABLE II.    ELECTRICAL PARAMETERS.

| Items | Rectangular coil | DD coil |
|---|---|---|
| $C_1$ | 160 nF | 0 |
| $C_{s2}$ | 162.5 nF | 94 nF |
| $C_{f1}$ | 270 nF | 49.7 nF |
| $C_{p2}$ | 150 nF | 142 nF |
| $V_{IN}$ | 380-500 V | 650-870 V |
| $V_{OUT}$ | 280-450 V | 280-420 V |

## C. Couplers

The charging pad consists of three layers: litz wire winding, ferrite cores, and aluminium plate. The topology of the winding determines the polarity of the produced magnetic field [6], [14]. When the coupler is optimized, a rectangular coil has a higher power transfer efficiency but it has an inferior misalignment tolerance in comparison to a DD coil with the same power density [15]. Therefore, SAE J2854 gives reference designs for both coil topologies. The outer dimensions of the winding embedded with ferrite cores are listed in Table III. The air gap is selected to be 170 mm that is much smaller than 10 meters. To ensure the accuracy of the FEM results, the infinite element method is applied to consider the open boundary as shown in Fig. 5. The resulting amplitude and phase of each pair of harmonic currents, for both the VA's and GA's currents, are assigned to coils and computed under the corresponding harmonic frequency.
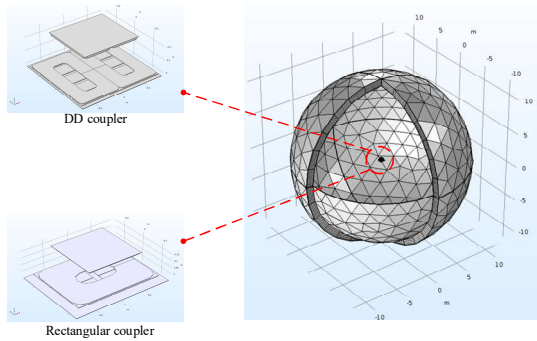


Figure 5. FEM model built in COMSOL

TABLE III.    EV CHARGING PADS DIMENSIONS.

| Class | Rectangular coil (mm) (L x W x H) | DD coil (mm) (L x W x H) |
|---|---|---|
| VA | 401.5 x 401.5 x 12.6 | 429 x 388 x 14.7 |
| GA | 750 x 510 x 25 | 630 x 590 x 22 |

## IV. RESULTS AND DISCUSSION

### A. Winding current harmonics

The total harmonics distortions (THD) and fundamental component of the winding current obtained from the circuit simulation are listed in Table IV. The winding current is obtained when the air gap is 170 mm, and the 11 kW output power is achieved.

All the simulated currents have a THD lower than 1%. In particular, the rectangular coil reference design suggests a

better performance than the DD coil. The VA's THD of the rectangular coil reference design is around a quarter that of the DD coil. In the primary LCC compensation circuit, the main coil, together with the series and parallel capacitor form a parallel resonant tank that is an excellent band-pass filter, and naturally attenuates well the harmonics components. As a consequence, the induced voltage and winding current on the secondary side contain few harmonics.

TABLE IV.    WINDING CURRENT.

| Items | Rectangular coil | | DD coil | |
|---|---|---|---|---|
| | GA | VA | GA | VA |
| $I_{1st}$ | 90.73 A | 66.67 A | 54.05 A | 63.39 A |
| THD | 0.25% | 0.18% | 0.59% | 0.66% |

The normalized amplitudes of the current harmonics are presented in Fig. 6. It can be seen from Fig. 6(a) and (c) that the odd orders are mostly larger than the adjacent even ones, and the third-order harmonics have the largest amplitude. The amplitude of harmonics drops below 0.1% when they are above the fifth order. When the frequency is higher than 1 MHz, the curves of the GA harmonics are consistently above that of the VA harmonics, as shown in Fig. 6(b) and (d).
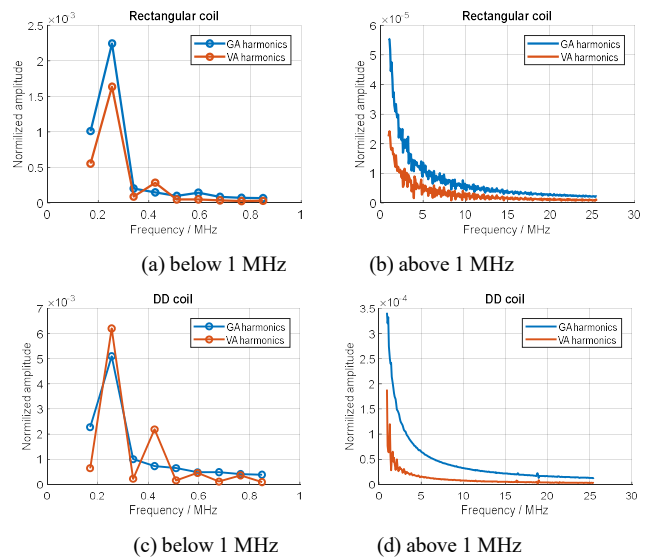


(a) below 1 MHz          (b) above 1 MHz

(c) below 1 MHz          (d) above 1 MHz

Figure 6. Current harmonics for reference design: (a) and (b) rectangular coil, (c) and (d) for DD coil.

TABLE V.    COILS' PARAMETERS.

| Items | | Rectangular coil | | DD coil | |
|---|---|---|---|---|---|
| | | Standards | FEM | Standards | FEM |
| $L_1$ ($\mu H$) | max | 38.7 | 39.373 | 71.7 | 70.551 |
| | min | 37.4 | 39.308 | 67.9 | 68.090 |
| $L_2$ ($\mu H$) | max | 40 | 40.819 | 64.7 | 63.887 |
| | min | 39.3 | 40.546 | 61.1 | 61.883 |
| $k$ | max | 0.229 | 0.1815 | 0.344 | 0.2496 |
| | min | 0.087 | 0.0947 | 0.14 | 0.1313 |
| $M$ ($\mu H$) | max | - | 7.269 | - | 16.757 |
| | min | - | 3.783 | - | 8.520 |

## B. Magnetic Field Radiation

In the standards SAE J2954, the Z3 air gap is defined as a range of 170 mm to 250 mm. Since the variation of air gap also affects the winding self-inductances, the value of $L_1$ and $L_2$ are recommended in a range which is presented together with the FEM results in Table V.

Generally, the listed parameters show an excellent agreement to the standards, which proves the reliability of the FEM model. The self-inductance of the DD coil locates within the range defined by the standards, while the mutual coupling is slightly lower. The self-inductances of the rectangular coil exceeds the range with an error of less than 1.74%, and the coupling coefficient is found within the range. Regarding the variation of the listed parameters, the coupling coefficients are more sensitive than that of the self-inductance. The maximum coupling coefficients nearly double that of the minimum in both designs. Besides, the coupling of the DD coil is twice larger than that of the rectangular coil.
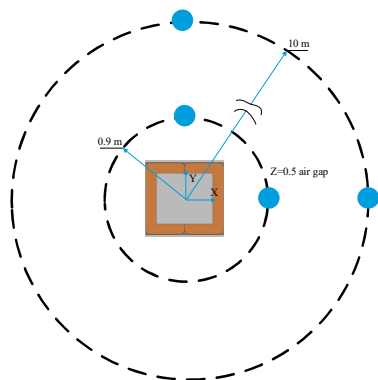


Figure 7. Locations of the investigated points



(a) Rectangular 10 meter points

(b) Rectangular 0.9 meters points

(c) DD 10 meter points
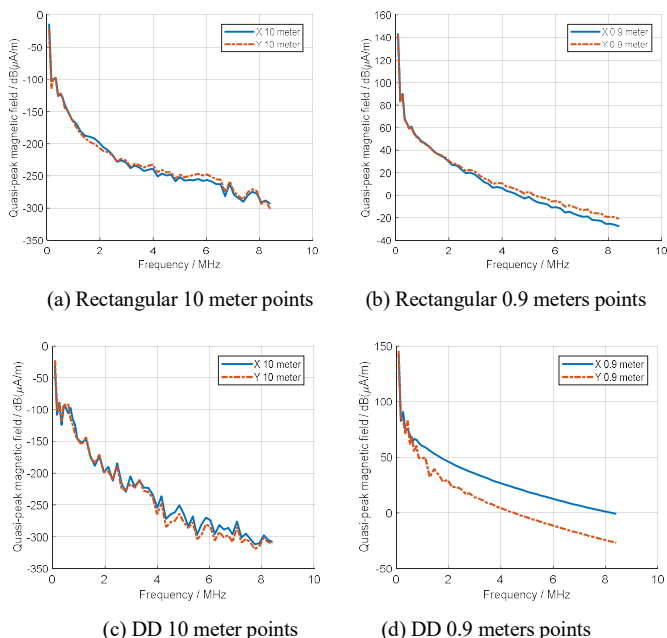
(d) DD 0.9 meters points

Figure 8. Quasi-peak value of the magnetic field radiated by the reference designs.

The relative locations of the investigated points are highlighted in Fig. 7. The magnetic fields radiated by the rectangular and DD coils reference designs are illustrated in Fig. 8. The trend and range of the magnetic field emission curves are similar in both analysed cases.

It can be seen from Fig. 8(a) and (b) that the magnetic field radiation is below 0 dB($\mu$A/m) and falls to minus 300 dB($\mu$A/m) at around 9 MHz. According to the limits in Fig. 2, the investigated two reference designs satisfy the magnetic field radiation requirement of SAE J2954. The margin at 10 meters point suggests that the power level of the reference designs can be increased further. However, due to the fact people, e.g., drivers or pedestrians, may stand close to an EV while this is being charged, compliance with the limits established by ICNIRP should be verified. According to the ICNIRP, the root-mean-square (RMS) value of the magnetic field density $B_{RMS}$ exposed to the general public should not exceed 27 $\mu$T. Based on (5), the equivalent quasi-peak value of the magnetic field intensity $H_{qp}$ is found around 149.66 dB ($\mu$A/m), when the permeability of the air is equal to $\mu_0$. The magnetic field radiation at a distance of 0.9 meters is presented in Fig. 8(b) and (d). As a result, the emission of both reference designs at the fundamental frequency is slightly below the limits. If these limits are required for the reference designs, better shielding methods should be applied before increasing the power level.

$$H_{qp} = 20\log_{10}(\sqrt{2}\frac{B_{RMS}}{\mu_0}10^6) \qquad (5)$$

## V. CONCLUSIONS

In this paper, two reference designs recommended in the standards SAE J2954 have been studied in terms of their magnetic field radiation. Based on the given electrical and mechanical specifications, the circuit and 3D FEM models were developed to analyse the winding current harmonics and respective magnetic field radiations under the proposed modelling assumptions. The results were compared with the limits defined in the standards, and it is found that the magnetic field radiation at a distance of 10 meters is considerably lower than the limits in SAE J2954, while the radiation at points of 0.9 meters away from the coupler is slightly lower than the limits defined by ICNIRP.

The parametric assumptions considered in the computational simulations are made to simplify the modelling approach, while the results may not accurately reflect the real situation. For example, the shielding effect of the EVs chassis is not yet modelled. Therefore, the simulated magnetic field radiations at 0.9 meters mostly tend to be larger than in real practice.

REFERENCES

[1] G. A. Covic and J. T. Boys, "Modern Trends in Inductive Power Transfer for Transportation Applications," *IEEE Journal of Emerging and Selected* Topics *in Power Electronics*, vol. 1, no. 1, pp. 28–41, Mar. 2013, doi: 10.1109/JESTPE.2013.2264473.

[2] C. C. Mi, G. Buja, S. Y. Choi, and C. T. Rim, "Modern Advances in Wireless Power Transfer Systems for Roadway Powered Electric Vehicles," *IEEE Transactions on Industrial Electronics*, vol. 63, no. 10, pp. 6533–6545, Oct. 2016, doi: 10.1109/TIE.2016.2574993.

[3] S. Kong *et al.*, "An Investigation of Electromagnetic Radiated Emission and Interference From Multi-Coil Wireless Power Transfer Systems Using Resonant Magnetic Field Coupling," *IEEE Transactions on Microwave Theory and Techniques*, vol. 63, no. 3, pp. 833–846, Mar. 2015, doi: 10.1109/TMTT.2015.2392096.

[4] C. Song *et al.*, "EMI Reduction Methods in Wireless Power Transfer System for Drone Electrical Charger Using Tightly Coupled Three-Phase Resonant Magnetic Field," *IEEE Transactions on Industrial Electronics*, vol. 65, no. 9, pp. 6839–6849, Sep. 2018, doi: 10.1109/TIE.2018.2793275.

[5] Seungyoung Ahn and Joungho Kim, "Magnetic field design for high efficient and low EMF wireless power transfer in on-line electric vehicle," in *Proceedings of the 5th European Conference on Antennas and Propagation (EUCAP)*, 2011, pp. 3979–3982.

[6] M. Budhia, J. T. Boys, G. A. Covic, and C. Huang, "Development of a Single-Sided Flux Magnetic Coupler for Electric Vehicle IPT Charging Systems," *IEEE Transactions on Industrial Electronics*, vol. 60, no. 1, pp. 318–328, Jan. 2013, doi: 10.1109/TIE.2011.2179274.

[7] W. Shi, J. Dong, S. Bandyopadhyay, F. Grazian, T. B. Soeiro, and P. Bauer, "Comparative Study of Foreign Object and Misalignment in Inductive Power Transfer Systems," in *IECON 2019 - 45th Annual Conference of the IEEE Industrial Electronics Society*, 2019, vol. 1, pp. 2634–2639, doi: 10.1109/IECON.2019.8926782.

[8] C.-S. Wang, O. H. Stielau, and G. A. Covic, "Design considerations for a contactless electric vehicle battery charger," *IEEE Transactions on Industrial Electronics*, vol. 52, no. 5, pp. 1308–1314, Oct. 2005, doi: 10.1109/TIE.2005.855672.

[9] Chwei-Sen Wang, G. A. Covic, and O. H. Stielau, "Power transfer capability and bifurcation phenomena of loosely coupled inductive power transfer systems," *IEEE Transactions on Industrial Electronics*, vol. 51, no. 1, pp. 148–157, Feb. 2004, doi: 10.1109/TIE.2003.822038.

[10] S. Zhou and C. C. Mi, "Multi-Paralleled LCC Reactive Power Compensation Networks and Their Tuning Method for Electric Vehicle Dynamic Wireless Charging," *IEEE Transactions on Industrial Electronics*, vol. 63, no. 10, pp. 6546–6556, Oct. 2016, doi: 10.1109/TIE.2015.2512236.

[11] F. Grazian, W. Shi, T. B. Soeiro, J. Dong, P. van Duijsen and P. Bauer, "Compensation Network for a 7.7 kW Wireless Charging System that uses Standardized Coils," in IEEE International Symposium on Circuits and Systems (ISCAS), 2020.

[12] F. Grazian, W. Shi, J. Dong, P. van Duijsen, T. B. Soeiro, and P. Bauer, "Survey on Standards and Regulations for Wireless Charging of Electric Vehicles," in *2019 AEIT International Conference of Electrical and Electronic Technologies for Automotive (AEIT AUTOMOTIVE)*, 2019, pp. 1–5, doi: 10.23919/EETA.2019.8804573.

[13] W. Zhang and C. C. Mi, "Compensation Topologies of High-Power Wireless Power Transfer Systems," *IEEE Transactions on Vehicular Technology*, vol. 65, no. 6, pp. 4768–4778, Jun. 2016, doi: 10.1109/TVT.2015.2454292.

[14] M. Budhia, G. A. Covic, J. T. Boys, and C. Huang, "Development and evaluation of single sided flux couplers for contactless electric vehicle charging," in *2011 IEEE Energy Conversion Congress and Exposition*, 2011, pp. 614–621, doi: 10.1109/ECCE.2011.6063826.

[15] S. Bandyopadhyay, P. Venugopal, J. Dong, and P. Bauer, "Comparison of Magnetic Couplers for IPT-Based EV Charging Using Multi-Objective Optimization," *IEEE Transactions on Vehicular Technology*, vol. 68, no. 6, pp. 5416–5429, Jun. 2019, doi: 10.1109/TVT.2019.2909566.